DISTANCE AND CAMERA FEATURE MEASUREMENTS AFFECT THE DETECTION OF TEMPERATURE ASYMMETRIES USING INFRARED THERMOGRAPHY

Álvaro S. Machado[1]; Mar Cañada-Soriano[2], Irene Jimenez-Perez[3,4]; Marina Gil-Calvo[3,5]; Felipe Pivetta Carpes[1]; Pedro Perez-Soriano[3]; Jose Ignacio Priego-Quesada[3,4*]

[1] Applied Neuromechanics Group, Laboratory of Neuromechanics, Federal University of Pampa, Uruguaiana, Brazil.

[2] Applied Thermodynamics Department (DTRA), Universitat Politècnica de València, Valencia, Spain

[3] Research Group in Sports Biomechanics (GIBD), Department of Physical Education and Sports, University of Valencia, Valencia, Spain.

[4] Research Group in Medical Physics (GIFIME), Department of Physiology, University of Valencia, Valencia, Spain.

[5] Faculty of health and sport sciences, Department of physiatry and nursing, University of Zaragoza, Huesca, Spain.

* Corresponding author

Jose Ignacio Priego Quesada. Ph.D.

Postal address: Department of Physical Education and Sports, Faculty of Physical Activity and Sport Sciences

St: Gascó Oliag, 3. 46010. Valencia, Spain.

e-mail: j.ignacio.priego@uv.es

Authors contributions

Conceptualization: all authors; Methodology: A.S.M., M.C-S., I.J.P, J.I.P-Q; Formal analysis and investigation: A.S.M., M.C-S., J.I.P-Q; Writing - original draft preparation: A.S.M., M.C-S., J.I.P-Q; Writing - review and editing: all authors; Resources: M.C-S., P.P-S., J.I.P-Q, ; Supervision: F.C., P.P-S., J.I.P-Q.

Word count (including tables, references and captions): 4811

Abstract

Small skin temperature asymmetries are claimed to indicate injuries, but the influence of measurement conditions and technical aspects of image acquisition are concerns for determining temperature asymmetries. This research determines whether distance and camera specifications affect thermal asymmetries detection. We simulated thermal asymmetries filling two glasses with water at different temperatures measured at two distances (0.7 and 1.5 m) using four different infrared cameras (T1020, E60BX, C2 and FLIR ONE). Linear regression verified the similarity between each camera and the T1020 camera (gold standard). The intraclass correlation coefficient assessed inter-camera reproducibility. Linear regression reported increasing adjustment using mean temperature, with lower values at 1.5 m between the T1020 and FLIR ONE (0.7 m, r= 0.58; 1.5 m, r= 0.34), C2 (0.7 m, r= 0.90; 1.5 m, r= 0.62) and E60BX (0.7 m, r= 0.96; 1.5 m, r= 0.68). Higher inter-camera reproducibility was observed at 0.7 m than 1.5 m. It is preferable to take thermal images with shorter distances and to prioritise cameras with superior hardware characteristics. The portability of FLIR ONE and C2 may be an advantage in studies investigating expected differences greater than 0.05 ºC and larger regions of interest.

Keywords: diagnostic imaging; injury; medicine; thermal asymmetries; thermal imaging; thermal sensitivity.

1.Introduction

Skin temperature symmetry is usually defined as the degree of similarity between the mean skin temperature of two Regions of Interest (ROIs) mirrored across the human body's longitudinal axis (1). Previous studies argue that a symmetrical skin temperature between human body sides could be assumed when absolute differences are lower than 0.5-0.7°C (1,2), while others suggested that asymmetries higher than 0.5-0.7°C could indicate physiological dysfunction related to pathologies and injuries. (3–5). The rationale behind the measurement of asymmetries in skin temperature involves a higher skin temperature of one body side being related to inflammation or higher vascularity, whereas a lower skin temperature is associated with nerve dysfunction or lower vascularity (3,6). Despite the criticism around the identification of a specific threshold for classifying asymmetries, the good reliability and reproducibility in the temperature asymmetries (7) leverage the growing interest in screening skin temperature symmetries as a strategy for the diagnosis and prevention of injuries (8,9).

Skin temperature can be determined using infrared thermography (IRT), a technique used in medical sciences since the 1960s (10). IRT has the advantage of being contactless and non-invasive (6), which made the tool of special interest in medicine, being a safe and easy to conduct measure for when carrying out follow-ups or screenings since it does not have any perjury on patients. The growing interest in applying IRT in the medical areas is benefited by the availability of reasonably affordable cameras, but with recognized low resolution (11). It results that the camera focal plane array size (FPA) can influence the detection of temperature asymmetries, since low FPA and/or high instantaneous field of view (IFOV) might not identify the small magnitudes of change in skin temperature associated with an skin temperature asymmetry (12). On the other hand, the concerns about camera quality and its impact on the field measurements is growing, motivating development of methods to improve camera resolution (13).

Another aspect of using IRT to determine thermal asymmetries is that camera FPA can affect the definition of the size of the regions of interest (ROI) from where temperature data are extracted, and therefore influence the detection of skin temperature asymmetries. ROI dimensions are limited by the distance between the measuring site and the camera (14). Although 25 pixels is recommended as the minimum size for properly defining a ROI (15), a larger ROI is always preferable (14,16). Furthermore, when analyzing asymmetries, the ROI from both body sides needs to be recorded within the same image, highlighting the role of camera FPA. However, when it comes to use in the clinical field, it is frequently important to measure the highest number of participants as fast as possible and therefore, higher distances between the camera and participants are performed (4) resulting in smaller ROIs, with few pixels than the recommended. From this point of view, the relationship between camera's hardware characteristics, ROI dimensions, and distance for image capture could influence estimation of skin temperature asymmetries.

The objective of this study was to determine whether distance and camera specifications affect the detection of thermal asymmetries. It has been hypothesized that at a larger distance, cameras with a lower FPA and a high IFOV could present a lower capacity to detect thermal asymmetries.

2. Methods

In this study, we compared four different IRT camera models from FLIR (FLIR, Wilsonville, Oregon, USA): T1020, E60BX, C2, and One Pro LT (FLIR ONE). All cameras work in the long-wave wavelength range (7-14μm) and their hardware characteristics are described in table 1. The correct calibration of the cameras was verified before the experiment started using a black body (BX-500 IR Infrared Calibrator, CEM, Shenzhen, China) (17,18).

Table 1. Hardware characteristics from the four thermographic cameras used in this study.

	T1020	E60BX	C2	FLIR ONE
Spectral range	7.5 – 14.0 μm	7.5 – 13 μm	7.5 – 14 μm	8 – 14 μm
FPA (Focal plane array)	1024 x 768	320 x 240	80 x 60	80 x 60
FOV (Field of view)	28° x 21°	25° × 19°	41° × 31°	50° x 38°
IFOV (Instantaneous field of view)	0.47 mrad	1.36 mrad	11 mrad	12 mrad
NETD*	< 20 mK	45 mK	100 mK	150 mK
Temperature range	-40°C to 150°C	–20°C to 120°C	–10°C to 150°C	-20°C to 120°C
Measurement uncertainty	± 2°C	± 2°C	± 2°C	± 5°C

*At 30°C. NETD: Noise Equivalent Temperature Difference.

Measurements were performed in a specialized laboratory for IRT measurements, in a space where environmental conditions were controlled (e.g. without light and airflow, with the room temperature controlled, and no person apart from the investigator in the measurement environment) (19). IRT measurements were obtained from water samples placed in two 115 x 65 mm glass crystallizers (Kavalierglass, Prague, Czech Republic) positioned at 0.7 m and 1.5 m far from the cameras. To produce temperature asymmetries, one of the glasses (G1) was filled with water (350 ml) and then heated to 40°C using a heater (Agimatic-E, JP Selecta, Barcelona, Spain). Immediately after reaching the target temperature, half of the water was poured into a second empty glass (G2), and both were placed on the ground, with 5 cm of distance in between, and in front of a black cloth to avoid the radiation reflection (3). Moreover, reflected temperature was measured according to the standard method ISO 18434-1:2008 and recorded in the camera settings. Because of the different transient temperature response from each glass, temperature asymmetries between them would be obtained as a result. Figure 1 illustrates the water temperature manipulation. To determine the temperature asymmetries, infrared images from all cameras were taken simultaneously obtaining the upper view of the glasses. For each of the cameras, images were recorded and compared every 30 s during 15 minutes. There were 5 sets of images obtained, with a 30-minute waiting period in between. For each set of photos, the process of heating the water and preparing the glasses was repeated. At first, the entire water heating and image-taking protocol was performed for the lowest height. Subsequently, the protocol was repeated for all data from the highest height. Regions of interest contained the water, in a upper view, and not included the glass region.

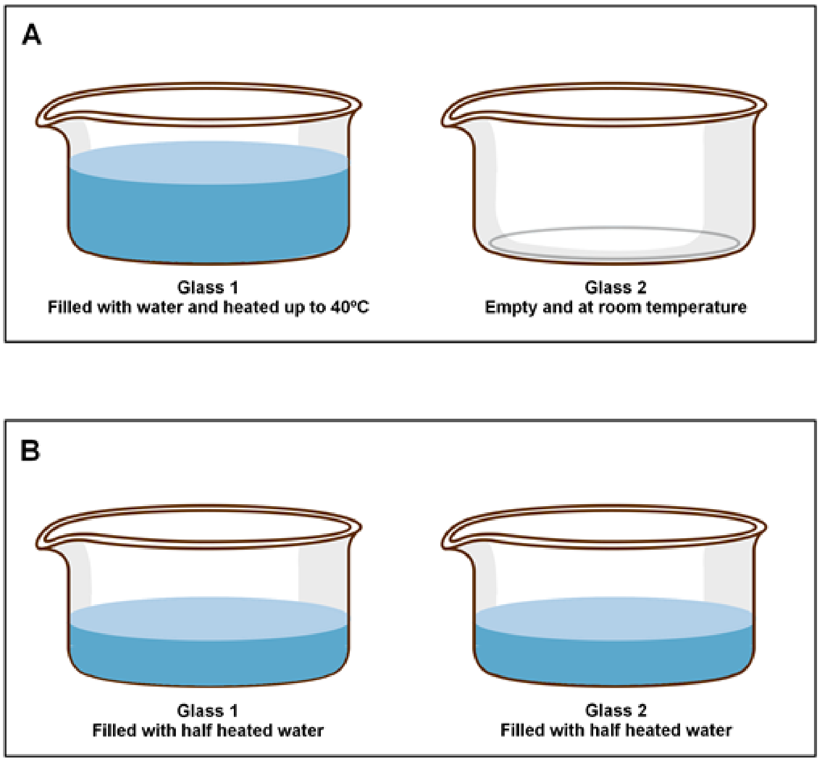

Figure 1. Firstly (A), the glass 1 was filled with water to be heated to 40°C, while the glass 2 remained empty at room temperature. Secondly (B), glass 2 was half filled with heated water. Infrared thermography images were taken for situation B.

All cameras were switched on for at least 10 minutes before acquiring the infrared images for electronic stabilization (19). Cameras T1020 and E60BX were mounted on tripods and programmed to acquire automatically images every 30 seconds for 15 minutes. On the other hand, cameras C2 and FLIR ONE were positioned and triggered manually, at the same distance from the glasses and following both the same time span between images and the 15 minutes recording period. Additionally, when C2 and FLIR ONE cameras were used, the image acquisition order was randomized for each trial.

The threshold defined to indicate temperature asymmetry was set at 0.5 °C, in agreement with previous studies addressing as this topic in medical studies threshold is usually considered in medicine for skin temperature (1,2). The values obtained by each T1020 camera's thermogram were used as a reference to define the existence of asymmetries for each time point (since the asymmetry would have a variable behavior over time) by simple subtraction of temperature between both glasses of water. The presence of false positives and/or negatives were verified, which means T1020 showing values lower than 0.5 °C, whereas values greater than 0.5 °C were obtained from any of the remaining cameras, and/or T1020 showing values greater than 0.5 °C, whereas lower values were obtained from any of the remaining cameras, respectively.

Infrared images were analyzed using a commercial thermography software (Thermacam Researcher Pro 2.10 software, FLIR, Wilsonville, USA). ROIs were defined as the total visible area of the water for each sample, excluding the glass itself, and mean and maximum temperature data were extracted. ROIs size of each camera at the distance of 0.7 m was: 88516 ± 1184 pixels for T1020, 8130 ± 171 for E60BX, 212 ± 20 for C2, and 8012 ± 798 for FLIR ONE. ROIs size at the distance of 1.5 m was: 16215 ± 254 pixels for T1020, 1976 ± 85 for E60BX, 37 ± 0 for C2, and 1511 ± 81 for FLIR ONE. On all cameras, emissivity was fixed at 0.97 for water surface temperatures (20,21). Figure 2 shows the arrangement of the data collection setup and the determination of ROI in the thermogram processing.

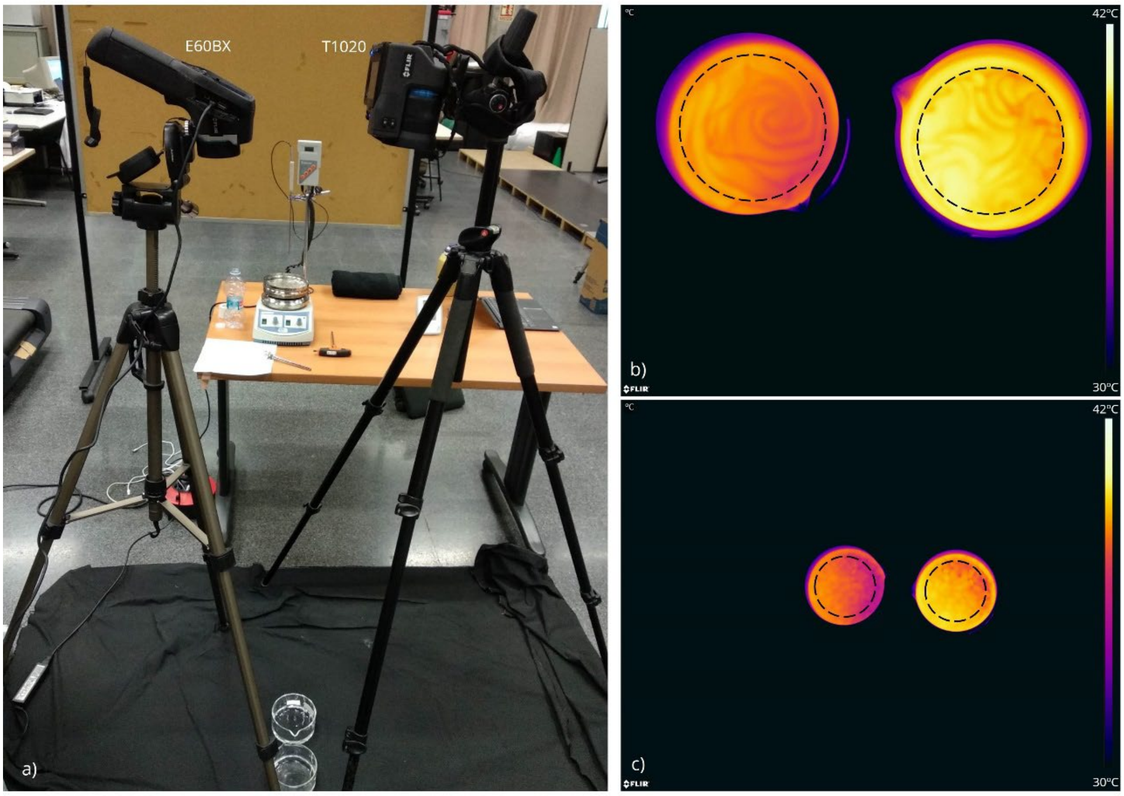

Figure 2. a) Experimental setup and thermal images performed with T1020 showing the ROIs (dashed lines) within the water in both glasses at b) 0.7 m and c) 1.5m.

Statistical analysis was performed using the software RStudio (version 1.2.5033). Linear regression analysis was performed to analyze the adjustment between T1020 and each camera for asymmetry calculation using mean and maximum temperature at the two distances. r-values, adjusted R^2, p-values, and equations of the adjustment were provided. Normal distribution of the residuals of the regressions models was verified ($p>0.05$) using the Kolmogorov-Smirnov test with Lilliefors correction. Bland-Altman plots were created to assess the agreement between T1020 and each of the other cameras, and to obtain the bias with 95% limits of agreement. Finally, the intraclass correlation coefficient was obtained to assess inter-camera reproducibility, based on a single rater-measurement, absolute-agreement, and 2-way random-effects model, between the T1020 and each of the other cameras for asymmetry calculation using mean and maximum temperature at the two distances. Intraclass correlation coefficients were classified from 1.00 to 0.81 as excellent reproducibility, 0.80 to 0.61 as very good reproducibility, 0.60 to 0.41 as good reproducibility, 0.40 to 0.21 as reasonable reproducibility, and 0.20 to 0.00 as poor reproducibility (22).

3.Results

Table 2 shows the percentage of false positives and negatives obtained for each camera. Percentages were higher for 1.5 m distances than for 0.7 m for all cameras. FLIR ONE presented the highest percentages of false negative using mean and maximum water temperature, and for both distances (>20%). At 1.5 m, C2 presented the highest percentages of false positives for mean and maximum water temperature (>15%).

Table 2. Percentage of false positives and negatives observed for mean and maximum temperatures for each camera and distance in comparison to the T1020 camera.

	Distance = 0.7 m			**Distance = 1.5 m**		
	E60BX	C2	FLIR ONE	E60BX	C2	FLIR ONE
			Mean temperature			
False Positive	0	4.4	0	14.7	21.6	7.8
False Negative	8.2	3.4	23.2	11.9	7.9	20.0
			Maximum temperature			
False Positive	0	0.6	1.7	12.6	15.8	4.3

False Negative	9.8	2.8	26.0	9.8	9.4	26.2

Linear regression analysis (Figure 3) reported increasing adjustment using mean temperature, with lower values at the 1.5 m, between the T1020 and FLIR ONE (distance 0.7 m, r= 0.58; distance 1.5 m r= 0.34), C2 (distance 0.7 m, r= 0.90; distance 1.5 m, r= 0.62), and E60BX (distance 0.7 m, r= 0.96; distance 1.5 m, r= 0.68). Similar results were observed using maximum temperature (Figure 4). Lower values were also found at 1.5 m, between the T1020 and FLIR ONE (distance 0.7, m r= 0.53; distance 1.5 m, R= 0.39), C2 (distance 0.7 m, r= 0.91; distance 1.5 m, r= 0.64), and E60BX (distance 0.7 m, r= 0.95; distance 1.5 m, r= 0.73).

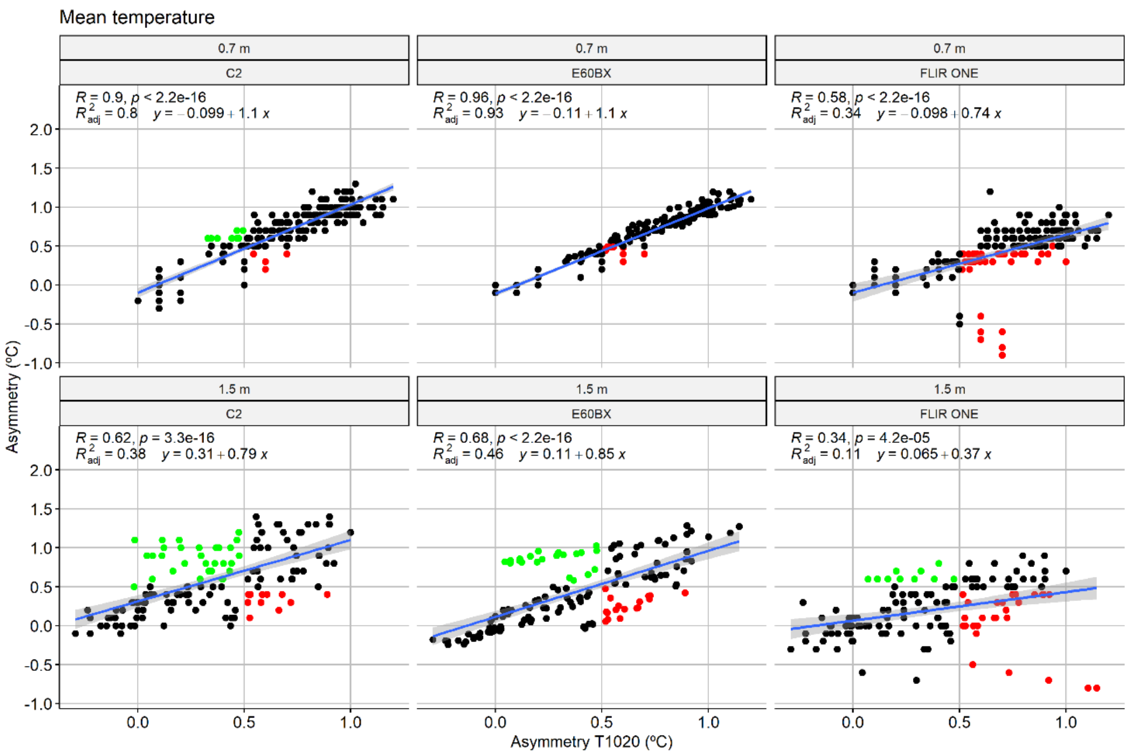

Figure 3. Linear regression analyses for the temperature asymmetry obtained at two camera distances (0.7 m and 1.5 m). False positives (green points) and negatives (red points).

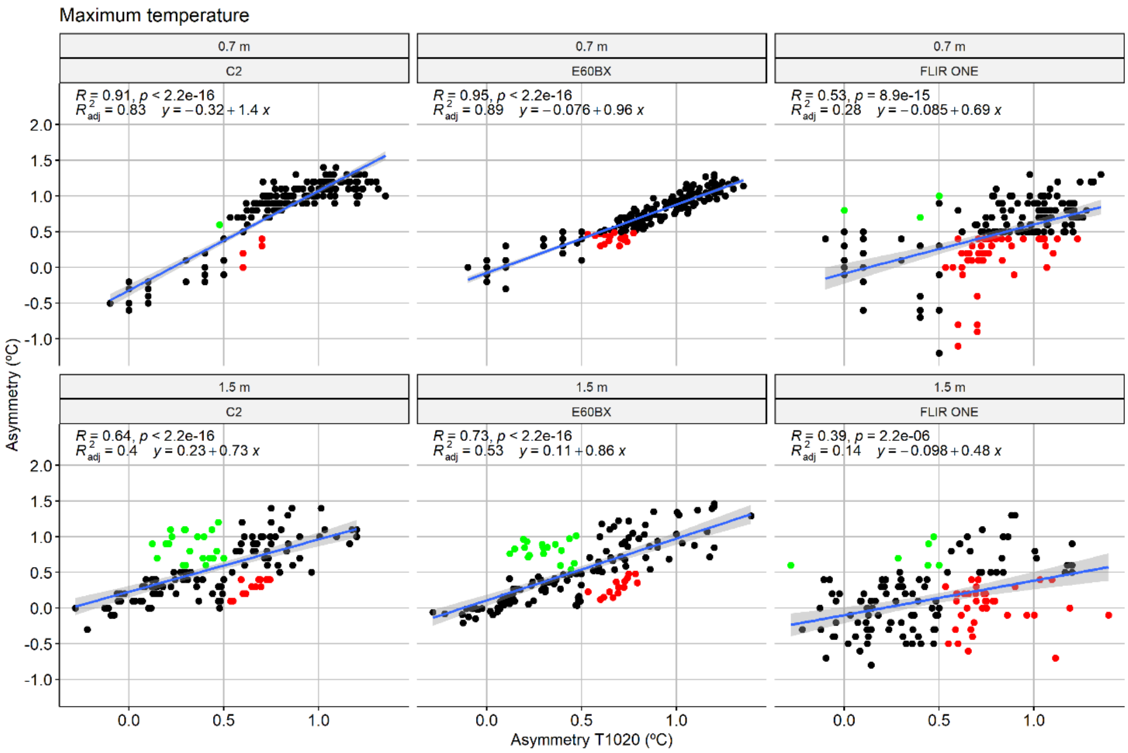

Figure 4. Linear regression analyses for the maximum temperature asymmetry obtained at two camera distances (0.7 m and 1.5 m). False positives (green points) and negatives (red points).

Bland Altman plots revealed increasing bias using mean temperature between the T1020 and E60BX, C2, and FLIR ONE at a distance of 0.7 m (Figure 5; bias: E60BX: 0.0 ±0.1 vs. C2: 0.0 ± 0.2 vs. FLIR ONE: 0.3 ± 0.3 °C). Higher biases were observed in distance of 1.5 m (bias: E60BX: -0.1 ± 0.3 vs. C2: -0.2 ± 0.3 vs. FLIR ONE: 0.2 ± 0.4 °C). Similar results were observed for maximum temperature (Figure 6; distance 0.7 m bias: E60BX: 0.1 ± 0.1 vs. C2: 0.0 ± 0.3 vs. FLIR ONE: 0.3 ± 0.4 °C; distance 1.5 m bias: E60BX: 0.0 ± 0.3 vs. C2: -0.1 ± 0.3 vs. FLIR ONE: 0.3 ± 0.4 °C).

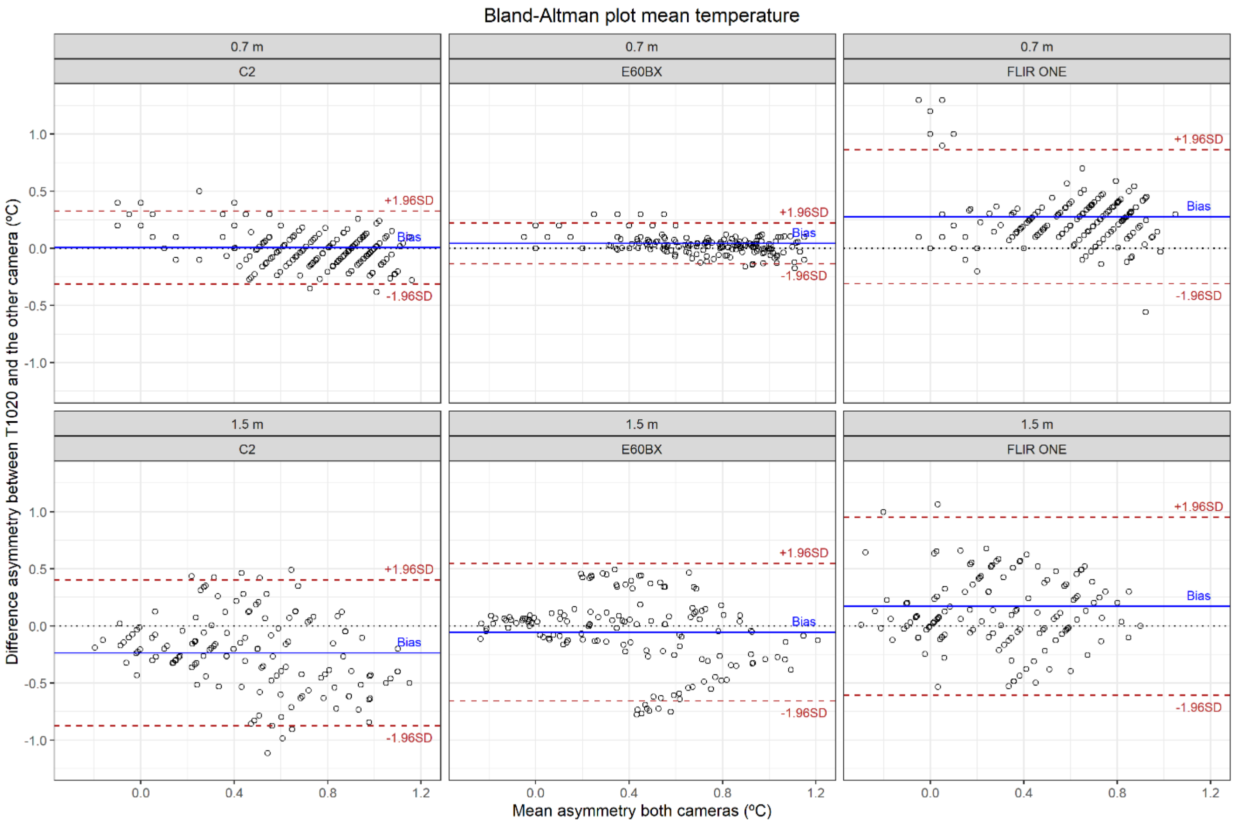

Figure 5. Difference of temperature asymmetry for the two distances (0.7 m and 1.5 m). Bland–Altman plots with 95% limits.

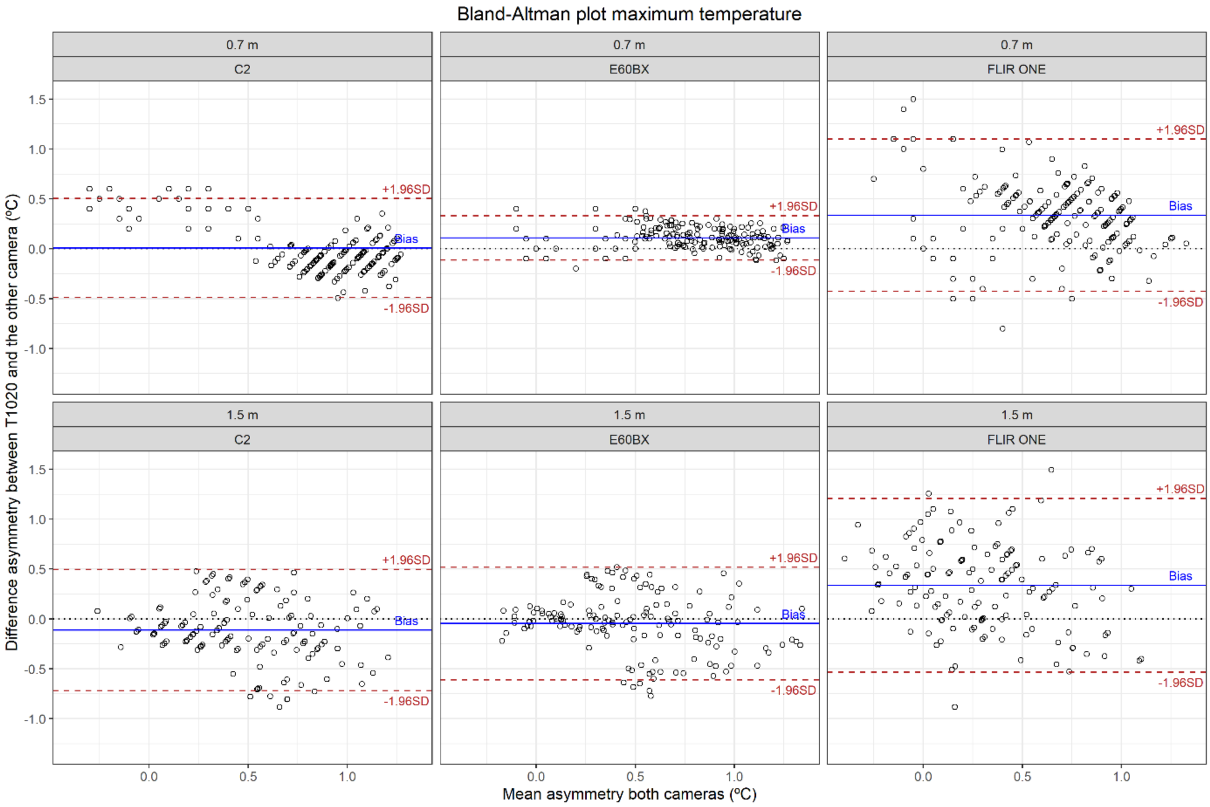

Figure 6. Difference of maximum temperature asymmetry for the two distances (0.7 m and 1.5 m). Bland–Altman plots with 95% limits.

Inter-camera reproducibility (Table 3) at a distance of 0.7 m was excellent for E60BX and C2 cameras, and moderately reasonable and good for FLIR ONE. At 1.5 m, the inter-camera reproducibility was very good for E60BX, moderately good and very good for C2, and reasonable for FLIR ONE.

Table 3. Intraclass correlation coefficients of inter-camera reproducibility between T1020 and the other three cameras for asymmetry calculation at two distances (0.7 m and 1.5 m).

	Distance = 0.7 m			**Distance = 1.5 m**		
	E60BX	C2	FLIR ONE	E60BX	C2	FLIR ONE
Mean	0.95 [0.90, 0.97]	0.87 [0.83, 0.90]	0.42 [0.01, 0.65]	0.66 [0.56, 0.74]	0.50 [0.16, 0.70]	0.30 [0.13, 0.45]
Maximum	0.90 [0.52, 0.96]	0.84 [0.79, 0.88]	0.38 [0.03, 0.61]	0.72 [0.63, 0.79]	0.60 [0.46, 0.71]	0.28 [0.02, 0.48]

4.Discussion

This study aimed to determine whether temperature asymmetry determination is affected by characteristics of four different thermographic cameras recording IRT images at two different distances from the region of interest. We set up an experiment considering measurements of water samples with temperature being manipulated to induce asymmetries of 0.5°C or higher, a reference often assumed as the cut-off point to discuss the relevance of temperature asymmetries (1,2,23). It was found that cameras of lower hardware characteristics (C2 and FLIR ONE) are more likely to present higher error rates.

In addition, the closer distance between the camera and the region of interest was a determining factor for the results' accuracy.

FPA influences the infrared camera performance (24). Considering T1020 as the reference camera, due to its FPA of 1020 x 768 pixels, E60BX camera (320 x 240 pixels) provided results, with a higher level of correlation with the reference camera (T1020). In the opposite direction, the other cameras (C2 and FLIR ONE), both with FPA of 80 x 60 pixels, showed higher false positives and negatives, a lower correlation index, and a greater bias for both maximum and mean temperatures, especially for the 1.5 m distance. FPA influences the ability to detail an image, especially at larger distances, and the FPA difference between cameras can determine a difference in temperature outcomes (11,12). It also affects the ROI delimitation. In our study, even though the images were circles with a relatively low level of demand to subjectively define de ROIs edges by the evaluator, images taken at 1.5 m still generated highly discrepant results in lower FPA cameras, which is in agreement with a previous study (18).

The distance between the camera and the region of interest may affect the accuracy of thermographic measurements. The measurements performed at 1.5 m generated higher levels of both false positives and negatives, including E60BX camera, which has better performance parameters. In a previous study, differences of up to 0.2 °C were found when thermographic measurements were conduct at 0.2 m and 2.5 m far from region of interest (26). In this study, where we used artificial samples and, therefore, free of intervening factors typical of experiments with humans (such as thermoregulation, sex, menstrual period, food, smoking, etc.), we further advance on the concept that even small variations in distance measurement can have an impact on the temperature outcomes, and invalidate discussions about asymmetries that show small magnitudes. Lower FPA cameras register images with less precision. It is important to be sure about the minimum region of interest dimension, which can be obtained by multiplying the camera's IFOV by the distance.

Bland Altman's graphics visually present that it is preferable to take pictures from shorter distances, and that the bias and scattering of results is overstated for the FLIR ONE camera, suggesting the possibility that data from this camera may result in misleading information. It is important to emphasize the effect of the distance between the camera and the region of interest on the results of IRT images, since there is a need to cover both legs within the image in some experiments, which end up leading to measurements at distances larger than 1.5 m between the camera and the region of interest (27,28).

FPA influences asymmetry determination, but it is important to note that even cameras with similar FPA may provide different results. The Noise Equivalent Temperature Difference (NETD), which quantifies the thermal sensitivity of the camera and also refers to the ability of the system to detect small temperature differences within the image, can be a source of differences between cameras with similar FPA. As lower is the NETD value, lower is the noise, and the smaller is the temperature differences that can be detected by the camera in an image (29).

Cameras with worse thermal sensitivity (higher NETD values at the same defined temperature) are less capable of avoiding false data homogeneity (30). It could impair the detection of relatively high temperature differences within the same thermogram, and therefore misleading injury diagnosis. The higher false negative rates found with cameras with worse thermal sensitivity, mainly the FLIR

ONE, could explain this limitation. The large amount of false positives in FLIR ONE results may also result of its overestimation of temperature (12), possibly producing images with false zones with heat peaks. Given that camera temperature ranges are related to NETD (31), when a certain temperature can be measured using two different temperature ranges, it would be advisable to select the narrowest one, since it would exhibit the lowest noise.

Although they are advantageous in terms of portability and low cost, the lack of adjustable focus in both the FLIR ONE and C2 cameras could be a disadvantage compared to the other cameras used in this research. Fixed focus prevents sharper thermograms and ROIs from being delineated, resulting in limitations for the distance between the camera and the region of interest (32). Although results with closer images indicate a low impact of the focal adjustment (33), we observed that the low sharpness of images taken at 1.5 m distance was determinant for inaccurate results.

In conclusion, cameras with better hardware characteristics produce accurate and consistent results in a wide range of practical situations. In these cases, both at maximum and mean temperature the results were solid, and the level of error as a function of distance was low. The C2 and FLIR ONE cameras have advantages such as portability, which can facilitate use in several situations including external environment and clinical setting. Their lower hardware characteristics may compromise the determination of temperature asymmetry results depending on the distance of image recording. These cameras may not be recommended for measures far than 0.7 m and for small ROIs (less than 25 pixels (15) or 3-4 times the IFOV (31)), for example in the analysis of diabetic foot (34).

The distance between the infrared camera and the sample also affects the results, and it is preferable to take a closer shot. Furthermore, cameras with superior hardware characteristics (e.g., ≥ 320 x 240 pixels, ≤ 1.3 mrad of IFOV or ≤ 45 mK of NETD) ensure greater data reliability when investigating thermal asymmetries of at least 0.5°C. For application fields with less need for precision (high size of ROIs and high asymmetries to detect), C2, which has the advantage of portability, seems to be sufficient.

A limitation of this study could be that the equations obtained have not been validated, for example employing a ROC curve (receiver operating characteristic curve) analysis with other data. However, our objective was not to use the equations, it was an approximation to know the degree of relationship between each camera and the T1020, as well as to evaluate the effect of distance on the detection of thermal asymmetries. Moreover, the asymmetries observed were dependent on the simulated situation created. We decided to use water to create asymmetries for its similar emissivity compared with the skin (water 0.97 vs. skin 0.98). However, another kind of simulation, for example using another liquid with different emissivity (e.g., oil), could modify the intensity of the differences observed. Finally, cameras present a considerable level of fluctuations and noise which can affect the results. Although this noise can be corrected by different computational methods (e.g., PCT, NMF, etc.), we want to reproduce the clinical conditions, and in these conditions, evaluators take the image and they did not do any of these corrections, except the calculation of the thermal asymmetry.

From an applied point of view, through the findings of this study we consider that researchers interested in evaluating thermal asymmetries may have better parameters to choose the most suitable thermographic cameras and will be able to observe that images taken closer present more consistent results. Altogether, this results also indicate that the standardization of the measurement protocols are a determining factor for the validity of analysis of temperature asymmetries.

Acknowledgments

FPC acknowledges the support from National Council for Scientific and Technological Development – CNPq – Brazil.

Funding details

ASM acknowledges funding from the Coordenação de Aperfeiçoamento de Pessoal de Nível Superior - Brasil (CAPES) - Finance Code 001.

Competing interests

The authors report there are no competing interests to declare.

6. References

1. Vardasca R, Ring EFJ, Plassmann P, Jones C. Termal symmetry of the upper and lower extremities in healthy subjects. Thermol Int. 2012 Apr 15;22:53–60.

2. Niu HH, Lui PW, Hu JS, Ting CK, Yin YC, Lo YL, et al. Thermal symmetry of skin temperature: normative data of normal subjects in Taiwan. Zhonghua Yi Xue Za Zhi Chin Med J Free China Ed. 2001 Aug;64(8):459–68.

3. Hildebrandt C, Raschner C, Ammer K. An Overview of Recent Application of Medical Infrared Thermography in Sports Medicine in Austria. Sensors. 2010 May 7;10(5):4700–15.

4. Fernández-Cuevas I, Arnáiz Lastras J, Escamilla Galindo V, Gómez Carmona P. Infrared Thermography for the Detection of Injury in Sports Medicine. In: Priego Quesada JI, editor. Application of Infrared Thermography in Sports Science [Internet]. Cham: Springer International Publishing; 2017 [cited 2021 Jun 2]. p. 81–109. (Biological and Medical Physics, Biomedical Engineering). Available from: http://link.springer.com/10.1007/978-3-319-47410-6_4

5. Sanchis-Sánchez E, Vergara-Hernández C, Cibrián RM, Salvador R, Sanchis E, Codoñer-Franch P. Infrared thermal imaging in the diagnosis of musculoskeletal injuries: a systematic review and meta-analysis. AJR Am J Roentgenol. 2014 Oct;203(4):875–82.

6. Priego Quesada JI, editor. Application of Infrared Thermography in Sports Science. 1st ed. 2017. Cham: Springer International Publishing : Imprint: Springer; 2017. 1 p. (Biological and Medical Physics, Biomedical Engineering).

7. Molina-Payá J, Ríos-Díaz J, Martínez-Payá J. Inter and intraexaminer reliability of a new method of infrared thermography analysis of patellar tendon. Quant InfraRed Thermogr J. 2021 Mar 15;18(2):127–39.

8. Côrte AC, Pedrinelli A, Marttos A, Souza IFG, Grava J, José Hernandez A. Infrared thermography study as a complementary method of screening and prevention of muscle injuries: pilot study. BMJ Open Sport Amp Exerc Med. 2019 Jan 1;5(1):e000431.

9. Gómez-Carmona P, Fernández-Cuevas I, Sillero-Quintana M, Arnaiz-Lastras J, Navandar A. Infrared Thermography Protocol on Reducing the Incidence of Soccer Injuries. J Sport Rehabil. 2020 Nov 1;29(8):1222–7.

10. Jones BF. A reappraisal of the use of infrared thermal image analysis in medicine. IEEE Trans Med Imaging. 1998 Dec;17(6):1019–27.

11. Machado ÁS, Priego-Quesada JI, Jimenez-Perez I, Gil-Calvo M, Carpes FP, Perez-Soriano P. Influence of infrared camera model and evaluator reproducibility in the assessment of skin temperature responses to physical exercise. J Therm Biol. 2021 May;98:102913.

12. Kirimtat A, Krejcar O, Selamat A, Herrera-Viedma E. FLIR vs SEEK thermal cameras in biomedicine: comparative diagnosis through infrared thermography. BMC Bioinformatics. 2020 Mar 11;21(Suppl 2):88.

13. Lai F, Kandukuri J, Yuan B, Zhang Z, Jin M. Thermal Image Enhancement through the Deconvolution Methods for Low-Cost Infrared Cameras. Quant Infrared Thermogr J. 2018;15(2):223–39.

14. Priego Quesada JI, Kunzler MR, Carpes FP. Methodological Aspects of Infrared Thermography in Human Assessment. In: Priego Quesada JI, editor. Application of Infrared Thermography in Sports Science [Internet]. Cham: Springer International Publishing; 2017 [cited 2021 Jun 2]. p. 49–79. (Biological and Medical Physics, Biomedical Engineering). Available from: http://link.springer.com/10.1007/978-3-319-47410-6_3

15. ISO (2009). Medical electrical equipment-deployment, implementation and operational guidelines for identifying febrile humans using a screening thermograph. TR 13154:2009 ISO/TR 8-600.

16. Bach AJ, Stewart IB, Minett GM, Costello JT. Does the technique employed for skin temperature assessment alter outcomes? A systematic review. Physiol Meas. 2015;36(9):R27.

17. Machin G, Simpson R, Broussely M. Calibration and validation of thermal imagers. Quant InfraRed Thermogr J. 2009 Dec;6(2):133–47.

18. Yoon ST, Park JC, Cho YJ. An experimental study on the evaluation of temperature uniformity on the surface of a blackbody using infrared cameras. Quant InfraRed Thermogr J. 2022 May 27;19(3):172–86.

19. Moreira DG, Costello JT, Brito CJ, Adamczyk JG, Ammer K, Bach AJE, et al. Thermographic imaging in sports and exercise medicine: A Delphi study and consensus statement on the measurement of human skin temperature. J Therm Biol. 2017 Oct;69:155–62.

20. Robinson PJ, Davies JA. Laboratory Determinations of Water Surface Emissivity. J Appl Meteorol Climatol. 1972 Dec 1;11(8):1391–3.

21. Rees WG, James SP. Angular variation of the infrared emissivity of ice and water surfaces. Int J Remote Sens. 1992 Oct;13(15):2873–86.

22. Weir JP. Quantifying Test-Retest Reliability Using the Intraclass Correlation Coefficient and the SEM. J Strength Cond Res. 2005;19(1):231.

23. Vainionpää M, Tienhaara EP, Raekallio M, Junnila J, Snellman M, Vainio O. Thermographic Imaging of the Superficial Temperature in Racing Greyhounds before and after the Race. Sci World J. 2012;2012:1–6.

24. Steketee J. Spatial resolution of thermographic cameras. Bibl Radiol. 1975;(6):25–32.

25. Liu G, Xia Y, Yang C, Zhang L. The Review of the Major Entropy Methods and Applications in Biomedical Signal Research. In: Zhang F, Cai Z, Skums P, Zhang S, editors. Hong Kong, City University of Hong Kong: Springer International Publishing; 2018. p. 87–100.

26. Danko M, Hudak R, Foffová P, Zivcak J. An importance of camera - subject distance and angle in musculoskeletal application of medical thermography. Acta Electrotech Inf. 2010 Jan 1;10.

27. Menezes P, Rhea MR, Herdy C, Simão R. Effects of Strength Training Program and Infrared Thermography in Soccer Athletes Injuries. Sports Basel Switz. 2018 Nov 19;6(4).

28. Adamczyk JG, Krasowska I, Boguszewski D, Reaburn P. The use of thermal imaging to assess the effectiveness of ice massage and cold-water immersion as methods for supporting post-exercise recovery. J Therm Biol. 2016 Aug;60:20–5.

29. Chrzanowski K, Bielecki Z, Szulim M. Comparison of temperature resolution of single-band, dual-band, and multiband infrared systems. Appl Opt. 1999 May 1;38(13):2820.

30. Obinah MPB, Nielsen M, Hölmich LR. High-end versus Low-end Thermal Imaging for Detection of Arterial Perforators. Plast Reconstr Surg Glob Open. 2020 Oct;8(10):e3175.

31. Vollmer M, Möllmann KP. Infrared Thermal Imaging: Fundamentals, Research and Applications [Internet]. Weinheim, Germany: Wiley-VCH Verlag GmbH & Co. KGaA; 2017 [cited 2021 Jun 8]. Available from: http://doi.wiley.com/10.1002/9783527693306

32. Okada K, Takemura K, Sato S. Investigation of Various Essential Factors for Optimum Infrared Thermography. J Vet Med Sci. 2013;75(10):1349–53.

33. Vogel B, Wagner H, Gmoser J, Wörner A, Löschberger A, Peters L, et al. Touch-free measurement of body temperature using close-up thermography of the ocular surface. MethodsX. 2016;3:407–16.

34. van Doremalen RFM, van Netten JJ, van Baal JG, Vollenbroek-Hutten MMR, van der Heijden F. Validation of low-cost smartphone-based thermal camera for diabetic foot assessment. Diabetes Res Clin Pract. 2019 Mar;149:132–9.

Figure captions

Figure 1. Firstly (A), glass 1 was filled with water to be heated to 40°C, while glass 2 remained empty at room temperature. Secondly (B), glass 2 was half filled with heated water. IRT images were taken for situation B.

Figure 2. a) Experimental setup and thermal images performed with T1020 showing the ROIs (dashed lines) within the water in both glasses at b) 0.7 m and c) 1.5m.

Figure 3. Linear regression analysis for the temperature asymmetry obtained in two camera distances (0.7 m and 1.5 m). False positives (green points) and negatives (red points).

Figure 4. Linear regression analysis for the maximum temperature asymmetry obtained in two camera distances (0.7 m and 1.5 m). False positives (green points) and negatives (red points).

Figure 5. Difference of temperature asymmetry in two distances (0.7 m and 1.5 m). Bland–Altman plots with 95% limits.

Figure 6. Difference of maximum temperature asymmetry in two distances (0.7 m and 1.5 m). Bland–Altman plots with 95% limits.